A Multi-QMOM Framework to Describe Multi-Component Agglomerates in Liquid Steel

L. Claudotte
ArcelorMittal Maizières Research S.A., RDMP, Maizières-lès-Metz 57283, France; and LEMTA, Nancy-University, CNRS, ESSTIN, Vandœuvre-lès-Nancy 54500, France

N. Rimbert
LEMTA, Nancy-University, CNRS, ESSTIN, Vandœuvre-lès-Nancy 54500, France

P. Gardin, M. Simonnet, and J. Lehmann
ArcelorMittal Maizières Research S.A., RDMP, Maizières-lès-Metz 57283, France

B. Oesterlé
LEMTA, Nancy-University, CNRS, ESSTIN, Vandœuvre-lès-Nancy 54500, France

DOI 10.1002/aic.12170
Published online January 20, 2010 in Wiley Online Library (wileyonlinelibrary.com).

A variant of the quadrature method of moments (QMOM) for solving multiple population balance equations (PBE) is developed with the objective of application to steel industry processing. During the process of oxygen removal in a steel ladle, a large panel of oxide inclusions may be observed depending on the type of oxygen removal and addition elements. The final quality of the steel can be improved by accurate numerical simulation of the multi-component precipitation. The model proposed in this article takes into account the interactions between three major aspects of steelmaking modeling, namely fluid dynamics, thermo-kinetics and population balance. A commercial CFD code is used to predict the liquid steel hydrodynamics, whereas a home-made thermo-kinetic code adjusts chemical composition with nucleation and diffusion growth, and finally a set of PBE tracks the evolution of inclusion size with emphasis on particle aggregation. Each PBE is solved by QMOM, the first PBE/QMOM system describing the clusters and each remaining PBE/QMOM system being dedicated to the elementary particles of each inclusion species. It is shown how this coupled model can be used to investigate the cluster size and composition of a particular grade of steel (i.e., Fe-Al-Ti-O). © 2010 American Institute of Chemical Engineers *AIChE J,* 56: 2347–2355, 2010

Keywords: liquid steel processing, ladle reactor, solid inclusion thermodynamics, population balance, growth, aggregation, quadrature method of moments

Introduction

Deoxidation and refining are steel processes that occur inside a ladle reactor of molten steel at 1600°C. They are specific instances of precipitation that have a large impact on the final steel quality since the production of some inclusions can create defects on future operations (stamping and rolling).[1]

During deoxidation a significant amount of oxide inclusions[2] are produced and the knowledge of their size and composition allows the steel quality to be controlled. Some studies[1–4] have shown that the typical elementary particle size of oxide inclusion ranges from nanometers to micrometers due to

Correspondence concerning this article should be addressed to N. Rimbert at nicolas.rimbert@esstin.uhp-nancy.fr.

growth and aggregation phenomena. A numerical tool has been developed to predict and to understand the production of large inclusions, taking into account the strong coupling between steel flow and chemical reactions. The spatial cluster evolution inside the ladle reactor is modeled by a CFD code (Fluent®) and the chemical composition evolution is computed using an in-house thermo-kinetic code.

Since McGraw[5] developed the quadrature method of moments (QMOM) and validated it for a problem of growth in an aerosol dynamics context, various developments have been achieved. Marchisio et al.[6,7] used QMOM for nucleation, crystal growth, and aggregation, and validated their results through comparison with some analytical results. However, as our study involves a large range of inclusion compositions, the standard QMOM is not appropriate because only one internal coordinate can be tracked. Here, a multi-QMOM model is presented, based on a decomposition of the global population balance equation (PBE), which involves several internal coordinates, into several PBE with one internal coordinate.

The main objective of this article is to present how the cluster size and composition are tracked by the multi-QMOM model. In the first part, the various PBE and the associated QMOM are described. Then the numerical implementation is detailed. The third part presents the numerical tool applied to a ladle reactor and results are finally discussed.

PBE and associated QMOM

In this section, the PBE and associated QMOM are presented. A new usage of QMOM for a multi-precipitation system with two or more different kinds of oxide is explained.

Original PBE

This study focuses on the three major particle behaviors that are observed inside a ladle reactor of liquid steel, namely nucleation, diffusion growth and aggregation. They can be expressed through a population balance model which is a continuity statement based on the number density function.

The time evolution of the particle size distribution (PSD) is described by the following equation based on the number density function in particle length coordinate:[6]

$$\frac{\partial n(L)}{\partial t}+\langle u_i\rangle\frac{\partial n(L)}{\partial x_i}-\frac{\partial}{\partial x_i}\left[\Gamma_t\frac{\partial n(L)}{\partial x_i}\right]=-\frac{\partial}{\partial L}[G(L)n(L)]+h(L), \tag{1}$$

where $n(L)$ is the number density function of particle size L, $\langle u_i\rangle$ denotes the Reynolds-averaged velocity in the x_i-direction (Einstein summation convention is applied), Γ_t is the turbulent diffusivity, $G(L)$ is the diffusion growth rate, and $h(L)$ represents the net rate of introduction of new particles into the system.[8] New particles of size L are originating from three source terms:

$$h(L)=J(L)+B(L)-D(L), \tag{2}$$

where $J(L)$ is the nucleation rate, $B(L)$ and $D(L)$ are the rate of birth and death, respectively, due to particle aggregation. According to the work of Smoluchowski (see the textbook by Ramkrishna[9]), we define the birth and death rates of aggregates for a discrete system composed of interacting monomers:

$$B(L)=\frac{1}{2}\int_0^L\frac{\beta\left(\left(L^3-\lambda^3\right)^{1/3},\lambda\right)}{\left(L^3-\lambda^3\right)^{2/3}}n\left(\left(L^3-\lambda^3\right)^{1/3}\right)n(\lambda)d\lambda, \tag{3}$$

$$D(L)=n(L)\int_0^\infty\beta(L,\lambda)n(\lambda)d\lambda, \tag{4}$$

where L and λ are particle sizes, β is the length-based aggregation kernel. Finally, neglecting the turbulent diffusion compared to the convective transport, the PBE can be rewritten as:

$$\frac{Dn(L)}{Dt}=-\frac{\partial}{\partial L}[G(L)n(L)]+J(L)+B(L)-D(L). \tag{5}$$

The left member of Eq. 5 regroups all the transport terms (D/Dt stands for the total derivative using the fluid velocity), whereas the right member represents the population size evolution.

PBE written in the QMOM framework

The moments of the PSD are obtained from the number density function by applying the moment transformation:

$$m_k=\int_0^\infty n(L)L^k dL, \tag{6}$$

where k is the moment order. The first four moments can be related to the physical properties of the distribution: m_0 is the number of particles per unit volume, m_1/m_0 is the mean diameter, m_2/m_0 is the mean particle surface area (up to a factor π for spherical particles), and m_3/m_0 is the mean particle volume (up to a factor $\pi/6$ for spherical particles).

As the left member of the PBE is solved using the CFD code, the terms in the right member must be approximated with the quadrature. Let us first apply the moment transformation for each term on the right-hand side:

$$\int_0^\infty\frac{Dn(L)}{Dt}L^k dL=\int_0^\infty kGn(L)L^{k-1}dL+JL^{*k}+B_k-D_k, \tag{7}$$

where L^* is the nucleus size, and

$$B_k=\frac{1}{2}\int_0^\infty n(\lambda)\int_0^\infty\beta(u,\lambda)\left(u^3+\lambda^3\right)^{k/3}n(u)dud\lambda, \tag{8}$$

$$D_k=\int_0^\infty L^k n(L)\int_0^\infty\beta(L,\lambda)n(\lambda)d\lambda dL, \tag{9}$$

with $u^3=L^3-\lambda^3$. The nucleation rate J and the crystal growth rate G are considered as time-dependent variables and their values are obtained by the thermo-kinetic software.

The QMOM can be seen as a moving class method where N_q classes evolve in size and weight. The so-called quadrature approximation is performed on the number density function:[6,7]

$$n(L)\approx\sum_{i=1}^{Nq}w_i\delta[L-L_i], \tag{10}$$

where N_q is the number of nodes, each of one is defined by its abscissa L_i and weight w_i, and δ is the Dirac delta function. The moments are obtained by using this Gaussian quadrature approximation in Eq. 6:

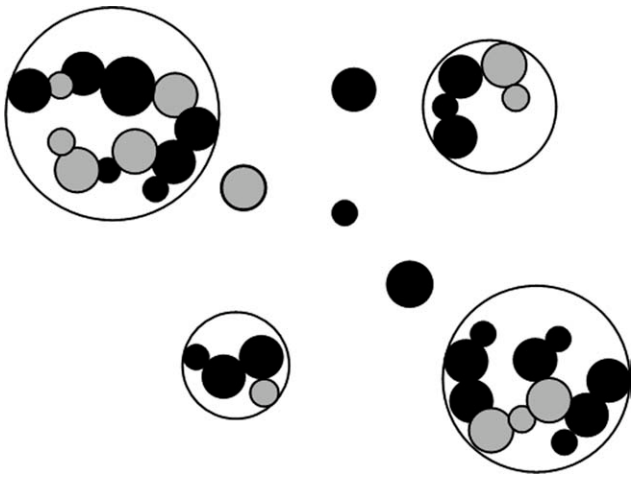

Figure 1. Symbolic representation of cluster shapes. Black and gray particles represent elementary particles belonging to two different phases.

These two species are followed by the elementary particle PBE/QMOM systems, while clusters are followed by the cluster PBE/QMOM system.

$$m_k = \int_0^\infty n(L)L^k dL \approx \sum_{i=1}^{N_q} w_i L_i^k. \tag{11}$$

The abscissas L_i and weights w_i are determined through the product-difference algorithm from the lower-order moments. Only $2N_q$ moments are needed to apply this algorithm.[5–7,10] Now, by applying the quadrature approximation in Eqs. 7–9 the moment equation becomes:

$$\frac{Dm_k}{Dt} = k\sum_{i=1}^{N_q} G(L_i)w_i L_i^{k-1} + JL^{*k} + \frac{1}{2}\sum_{i=1}^{N_q} w_i \sum_{j=1}^{N_q} w_j \left(L_i^3 + L_j^3\right)^{k/3} \times \beta_{ij} - \sum_{i=1}^{N_q} L_i^k w_i \sum_{j=1}^{N_q} w_j \beta_{ij}, \tag{12}$$

where $\beta_{ij} = \beta(L_i, L_j)$. It has been shown[6,7] that it is possible to track with high accuracy the moments of the PSD by using only three nodes ($N_q = 3$).

Multi-PBE model description

To better understand the issues of this project, a symbolic representation of the shape and composition of the harmful inclusions is displayed in Figure 1.

The particle size depends on the critical nucleation length L^*, on the diffusion growth rate G, on the rate of aggregation β_{ij} and obviously on the nature of inclusions produced inside the reactor. From this description, it is obvious that several internal coordinates are necessary to properly describe the shape and composition of clusters.

Recently, Marchisio and Fox[11–13] developed the method of direct quadrature of moments (DQMOM) to solve the PBE with two or more internal coordinates, however this method still suffers from some numerical instability. This is especially true when a large number of internal coordinates is required, mainly due to ill-conditioned matrices and to the difficulty of choosing the right set of moments. Thus, for the time being, the DQMOM has been excluded for the present application. By contrast, the QMOM with one internal coordinate is a precise approximation of the original PBE.

Accordingly, an alternate method relying solely on QMOM has been devised. The presented multi-QMOM method does not take the correlations between composition and size into account. In this manner, the chemical composition is followed by using a QMOM/PBE system for each kind of precipitate (i.e., Al_2O_3, TiO_2…). Each system follows the number of nuclei ($m_{0,p}$) and the size of the elementary particles for the precipitate p. In return, only diffusion growth and nucleation can modify the distribution:

$$\frac{Dm_{k,p}}{Dt} = k\sum_{i=1}^{N_q} G_{i,p} w_{i,p} L_{i,p}^{k-1} + J_p L_p^{*k}, \tag{13}$$

where the subscript p stands for the elementary particle PBE/QMOM system. Then, the cluster size is followed by a dedicated PBE/QMOM system which includes all elementary particles, with a particular growth treatment based on volume conservation and a particle collision calculation:

$$\frac{Dm_{k,c}}{Dt} = k\sum_{i=1}^{N_q} G_{i,c} w_{i,c} L_{i,c}^{k-1} + \sum_{p=1}^{N_p} J_p L_p^{*k} + \frac{1}{2}\sum_{i=1}^{N_q} w_{i,c} \sum_{j=1}^{N_q} w_{j,c} \times \left[\left(L_{i,c}^3 + L_{j,c}^3\right)^{\frac{k}{3}} - L_{i,c}^k - L_{j,c}^k\right]\beta_{ij}, \tag{14}$$

where N_p is the number of precipitated phases, $G_{i,c}$ is the diffusion growth rate of the cluster envelope and the subscript c stands for the cluster PBE/QMOM system. The nucleation term in Eq. 14 comes from the PBE/QMOM system for elementary particles. All new nuclei are considered as clusters with only one particle that can collide with other particles to grow up.

Multi-QMOM results

The multi-QMOM has been developed to obtain the cluster size and composition inside a liquid steel ladle from a single simulation.

The mean cluster or particle size is observed by tracking the Sauter mean diameter $d_{32,c} = m_{3,c}/m_{2,c}$ or $d_{32,p} = m_{3,p}/m_{2,p}$. We also define the number-volume mean diameter $d_{30,c}$:

$$d_{30,c} = \sqrt[3]{\frac{m_{3,c}}{m_{0,c}}} \tag{15}$$

Then, the elementary particle PBE and the cluster PBE are linked by a volume conservation hypothesis, which implies that the global precipitate volume is equal to the total cluster volume. This yields the following relationship between all third-order moments:

$$m_{3,c} = \sum_{p=1}^{N_p} m_{3,p}. \tag{16}$$

The cluster size and cluster composition can be assumed to be independent of each other provided that collisions do not depend on the type of oxide. This assumption is realistic because alumina and titanium oxides are considered as solid spherical particles. The volume percentage of one oxide p inside a cluster is defined by:

$$\phi_{v,\mathrm{p}} = \frac{m_{3,\mathrm{p}}}{m_{3,\mathrm{c}}}. \tag{17}$$

Finally, the average mass of a cluster is written by using the parameters defined in Eqs. 15 and 17:

$$M_{\mathrm{cluster}} = \sum_{p=1}^{N_\mathrm{p}} k_\mathrm{v} \rho_\mathrm{p} \phi_{v,\mathrm{p}} \left(d_{30,\mathrm{c}}\right)^3, \tag{18}$$

where k_v is the volume shape factor (equal to $\pi/6$ for spherical particles) and ρ_p is the oxide density.

Numerical Implementation

Coupling fluid motion, chemistry, and population balance

The software is made up of three independent pieces of software that can share data through file access. The chemical composition and all the moment vectors are transported as passive scalars inside the Fluent® CFD software. The chemical composition is sent to the thermo-kinetic code once the scalar transport computation has been achieved by the CFD code. The thermo-kinetic software checks the chemical equilibrium evolution and computes the growth and nucleation rates for each precipitate. The chemical composition is then sent back to the CFD code. Finally, all moments of PBE/QMOM systems are updated with terms stemming from diffusion growth, elementary particles nucleation and aggregation (actually only for the clusters PBE), making the coupling process ready for a new time-step. As QMOM is directly implemented in the CFD code Fluent®, in the form of user defined functions, the variables are shared by the two programs. The thermo-kinetic code is called as an external application and it exchanges data with the CFD code through ASCII data files.

Nucleation and diffusion growth rates

The nucleation rate J and the diffusion growth rate G are computed by the thermo-kinetic code, which is based, according to the classical nucleation theory (CNT), on the minimization of the Gibbs free energy. The competition between the volumic nucleation driving force and the surface creation energy cost results in a minimum given by Ref. 14:

$$\Delta G^* = \frac{16\pi\sigma^3}{3\ \Delta G_v^2}, \tag{19}$$

where σ is the interfacial energy, and ΔG_v is obtained from

$$\Delta G_v = I\left(\sum_{i,j} C_{ji} X_i\right)/V_m, \tag{20}$$

with I denoting the driving force of precipitation. C_{ij} is the number of atoms of component j in the oxide i, X_i is the mole fraction of oxide i and V_m is the oxide mole volume. For a given oxide stoichiometric compound, the driving force I obeys the following expression:

$$I = RT \ln\left\{\left(\frac{(a_\mathrm{E})^x (a_\mathrm{O})^y}{K_{\mathrm{E}_x\mathrm{O}_y}.a_{\mathrm{E}_x\mathrm{O}_y}}\right)^{\frac{1}{x+y}}\right\}, \tag{21}$$

where R is the ideal gas constant, T denotes temperature, a_E and a_O are, respectively, the activities of element E and of oxygen referred to the 1% dilute solution, $a_{\mathrm{E}_x\ \mathrm{O}y}$ is the activity of $\mathrm{E}_x\mathrm{O}_y$ in the oxide, $K_{\mathrm{E}_x\ \mathrm{O}y}$ is the solubility product of $\mathrm{E}_x\mathrm{O}_y$ in the liquid metal, and x and y are the appropriate stoichiometric coefficients. Then the rate of homogeneous nucleation of inclusions is given by:

$$J = Z\beta_n N_s \exp\left(-\frac{\Delta G^*}{k_\mathrm{B} T}\right), \tag{22}$$

where Z is the Zeldovitch factor, β_n a frequency factor, N_s the number of nucleation sites per unit volume, and k_B the Boltzmann constant.

In the thermo-kinetic software, it is considered that all precipitates are spherical with the diameter of new nuclei, increasing for decreasing driving force according to CNT, given by

$$L^* = -4\sigma/\Delta G_v, \tag{23}$$

therefore the nucleus diameter is larger at the end of the process than at the beginning.

Finally, when the diffusion growth rate is not limited by interfacial kinetics the diffusion flux at the surface is obtained as follows:

$$\Phi_i = k_i\left(C_i^{(l)} - C_i^{(i)}\right), \tag{24}$$

where $C_i^{(l)}$ and $C_i^{(i)}$ are the concentrations in mol m^{-3}, respectively in the liquid steel far from the precipitate and at the interface. $C_i^{(l)}$ is given by composition transport and when the growth is controlled by diffusion, $C_i^{(i)}$ is the equilibrium value. Here, due to the small size of the precipitates, the Sherwood number $2rk_i/D_i$ can be assumed equal to two, therefore the mass transfer coefficient k_i is taken equal to D_i/r where D_i is the diffusion coefficient of the element i and r the radius of the precipitate (cf. Table 1).

Growth treatment for elementary particles

Instead of directly using the diffusion growth rate $G_{p,i}$ presented in Eq. 13 where the weights of the Dirac's distributions are modified accordingly, the abscissas are shifted

Table 1. Values of Density and Diffusion Coefficients in Liquid Steel at 1873 K

	Units	Steel
ρ	kg m^3	7.00×10^3
μ	Pa s	6.2×10^{-3}
D_{Al}	$\mathrm{m}^2\ \mathrm{s}^{-1}$	3.02×10^{-9}
D_{O}	$\mathrm{m}^2\ \mathrm{s}^{-1}$	12.58×10^{-9}
D_{Ti}	$\mathrm{m}^2\ \mathrm{s}^{-1}$	8.3×10^{-9}

ensuring growth in a proper manner. Let us describe more precisely this procedure in the following. First, the oxide volume is connected to the third moment according to the following relationship:

$$V_{i,p} = k_v w_{i,p} L_{i,p}^3. \tag{25}$$

Then, we notice that only the size of the particles (and not their number) is concerned by diffusion growth, so that it is useless to try to modify the weights (i.e., the number of the moving classes of the QMOM framework). The volume variation for node i during a time-step Δt is obtained through:

$$\Delta V_{i,p} = k_v \Delta\left(w_{i,p} L_{i,p}^3\right) = k_v w_{i,p}\left(L_{i,p}^3(t+\Delta t) - L_{i,p}^3(t)\right), \tag{26}$$

giving finally the new abscissa used to reconstruct the vector of moments for the next time-step:

$$L_{i,p}(t+\Delta t) = L_{i,p}(t)\left[1 + \frac{\Delta V_{i,p} k_v^{-1}}{w_{i,p} L_{i,p}^3(t)}\right]^{1/3}. \tag{27}$$

As a consequence, the product-difference algorithm is not used because the new treatment of particle diffusion growth only shifts the node abscissas. It may be noticed that even if this new way of treating the particle growth may seem quite simple, it is an important modeling step as it enforces the numerical stability. Actually, it has been observed that if weights and abscissas were modified as presented in Eq. 14, the product-difference algorithm might fail. Therefore, the set of moments obtained (and convected) thereafter is still the set of moments of a real distribution.

Growth treatment for clusters

Even if the problem has been simplified by decoupling the cluster size from the cluster composition, i.e., $n_{\text{Cluster}}(L,X_1,\ldots X_p) \approx n_{\text{Cluster}}(L)$, the cluster volume must satisfy the volume conservation hypothesis. In the same way that the diffusion growth of elementary particle is treated, the QMOM abscissas of clusters are shifted using a multiplying factor h_f. Consequently, the new cluster QMOM abscissas are calculated as follows:

$$L_{i,c}(t+\Delta t) = L_{i,c}(t) h_f, \tag{28}$$

with a factor independent of the abscissa:

$$h_f = \left(1 + \frac{\Delta m_{3,c}}{m_{3,c}}\right)^{1/3}. \tag{29}$$

To illustrate the described model for cluster growth, Figure 2 shows the impact of h_f upon a Gaussian cluster shape with a QMOM using four nodes. Therefore, for a global volume divided by two ($h_f = 2^{-1/3} \approx 0.794$) or multiplied by two ($h_f = 2^{1/3} \approx 1.259$), the global shape of the cluster population is conserved and only abscissas are modified in accordance with the volume conservation hypothesis.

The two models for elementary particle growth or cluster growth are nearly the same, as shown by Eqs. 27 and 28.

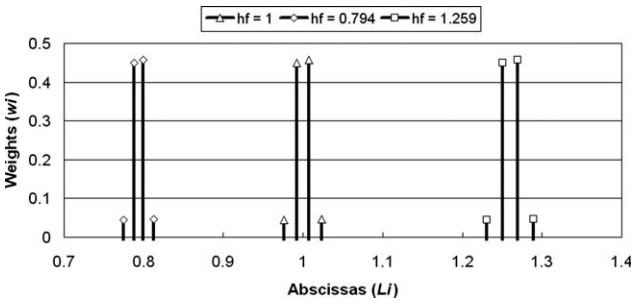

Figure 2. Shape evolution due to cluster growth model (Gaussian initialization, four nodes).

Let us point out that the growth coefficient for elementary particles is computed node by node whereas there is only one coefficient for clusters.

Aggregation kernel

In this article, the aggregation mechanism is classically assumed to be a second-order process, in which the rate of collision is proportional to the product of concentrations of the two colliding species.[15] Thanks to dilution, the collisions between three bodies or more are neglected. Moreover, as the collisions are assumed to be instantaneous, a three-body collision can be considered as the succession of two binary collisions. Three kernels are used, according to their range of influence:

- For very small particles (negligible inertia), Brownian motion is the main mechanism leading to inter-particle collisions; in this case, the kernel writes as:

$$\beta_{ij}^{\text{Br}} = \frac{2k_B T}{3\mu_L}\frac{\left(R_{c,i} + R_{c,j}\right)^2}{R_{c,i} R_{c,j}}, \tag{30}$$

where $R_{c,i} = L_i/2$ is the collision radius and μ_L is the fluid viscosity.

- For inertial particles that do not perfectly follow the turbulent fluctuations, the effect of Brownian motion can be neglected, and turbulence becomes the main mechanism; if the particle diameter is smaller than the Kolmogorov microscale, $\eta_K = (\nu_L^3/\varepsilon)^{1/4}$, a new collision kernel can be used. The turbulent aggregation kernel can be expressed by

$$\beta_{ij}^{\text{Turb}} = \alpha\left(R_{c,i}, R_{c,j}\right)\beta_{ij0}^{\text{Turb}} = \alpha\left(R_{c,i}, R_{c,j}\right)\sqrt{\frac{8\pi}{15}\frac{\varepsilon}{\nu_L}}\left(R_{c,i} + R_{c,j}\right)^3, \tag{31}$$

where $\beta_{ij0}^{\text{Turb}}$ is the Saffman-Turner collision kernel[16] and $\alpha(R_{c,i}, R_{c,j})$ is the coagulation efficiency, which takes into account the forces to eliminate the liquid film between two colliding particles and the Van der Waals force.[17,18] It can be shown that the Brownian kernel alone generally does not lead to rapid formation of large aggregates and that the turbulent kernel significantly enhances the rate of inter-particle collisions.[15]

- If precipitates are lighter than the liquid, then collisions happen due to the difference in rise velocities between particles of various size. The corresponding Stokes aggregation kernel is given by:

$$\beta_{ij}^{\mathrm{St}} = \alpha\left(R_{c,i}, R_{c,j}\right)\beta_{ij0}^{\mathrm{St}} = \alpha\left(R_{c,i}, R_{c,j}\right)\frac{2\pi g\left(\rho_L - \rho_p\right)}{9\mu_L}\left|R_{c,i}^2 - R_{c,j}^2\right| \left(R_{c,i} + R_{c,j}\right)^2, \quad (32)$$

where g denotes the gravitational acceleration.

In Eqs. 31 and 32 the coagulation efficiency is expressed in terms of the mean velocity gradient $\dot{\gamma}$ in the particle neighborhood, following Van de Ven and Mason[18]:

$$\alpha\left(R_{c,i}, R_{c,j}\right) = 0.8H^{0.18}\left(36\pi\mu_L\dot{\gamma}\left(\frac{R_{c,i} + R_{c,j}}{2}\right)^3\right)^{-0.18}, \quad (33)$$

where H is the Hamaker constant, the value of which is not well established for the mixed oxides studied here. Therefore H is set to 10^{-20} J in the next simulation, a value which is a good compromise with predicted values obtained for Al_2O_3 alone in liquid iron at $T = 1873$ K ($H = 2.3 \times 10^{-20}$ J).[19] For the Saffman-Turner kernel, the mean velocity gradient in Eq. 33 is $\dot{\gamma} = \sqrt{\varepsilon/\nu_L}$, while in case of Stokes collisions the velocity gradient is obtained from the difference in terminal velocities of two particles:

$$\dot{\gamma} = \frac{2g}{9\mu_L}\left|\rho_L - \rho_p\right|\frac{\left|R_{c,i}^2 - R_{c,j}^2\right|}{R_{c,i} + R_{c,j}} = \frac{2g}{9\mu_L}\left|\rho_L - \rho_p\right|\left|R_{c,i} - R_{c,j}\right|. \quad (34)$$

As is usual, the aggregation kernel is finally approximated by simply adding the three kernels given by Eqs. 30–32:

$$\beta_{ij} = \beta_{ij}^{\mathrm{Br}} + \beta_{ij}^{\mathrm{Turb}} + \beta_{ij}^{\mathrm{St}}. \quad (35)$$

Time stepping for aggregation

The solution of multi-QMOM/PBE is split into three parts: nucleation, growth by diffusion and growth by aggregation. To ensure positive values of the three first moments using an Euler time integration scheme, the aggregation source term is calculated with the following general time step condition:

$$\Delta t_0 \le K\frac{m_0(t)}{D_0 - B_0}, \quad (36)$$

where K is a constant defining the cluster aggregation limitation (e.g., for $K = 0.005$, only 0.5% of the population are aggregated), and B_0, D_0 are the birth and death source terms for the moment m_0, according to Eqs. 8 and 9. Note that $D_0 > B_0$, so that all terms in Eq. 36 are positives. As shown in Figure 3, the general time step condition is validated by the comparison between analytical and numerical results, assuming an exponential initial PSD for a constant aggregation kernel β_0:

$$m_k(t) = m_k(t=0)\left(\frac{2}{2 + N_0\beta_0 t}\right)^{1-k/3} \quad (37)$$

where N_0 is the initial number of particles per unit volume (m^{-3}). The moments are initialized with the gamma function Γ:

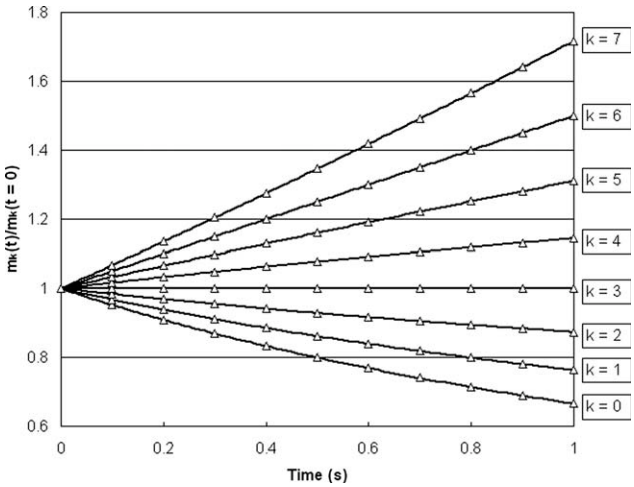

Figure 3. Aggregation validation case: N_0 = 1/m^3 and β_0 = 1 m^3 s^{-1}.

Symbols: analytical solution; solid lines: numerical solution obtained with four nodes.

$$m_k(t=0) = \Gamma\left(1 + \frac{k}{3}\right). \quad (38)$$

The same aggregation test case has been performed in a one-dimensional simulation by transforming the time dependent PBE into a steady one-dimensional PBE with a uniform convection velocity[20] ($u = 1$ m s^{-1}). Results obtained by this simulation, using the same initialization, are also in good agreement with the analytical solution.

Application to a Model Ladle Reactor

Geometry and simulation set up

The ladle reactor (Figure 4) is a cylindrical vessel lined with refractory bricks and stirred with argon bubbles injected through a porous bumper at the bottom center. On top of the liquid steel, the slag protects the steel from reoxidation by the air oxygen and from heat losses. It also captures solids inclusions. A ladle of height $h = 3.70$ m and radius $r = 2$ m contains about 325 tons of liquid steel. To reduce computational cost, a two-dimensional axisymmetric geometry is modeled in this work, and the energy equation is not solved, which means that neither the heat losses through the ladle walls and surface nor the heat production by precipitation are taken into account. In the present state, the slag is modeled as a reflecting wall without inclusion extraction or chemical exchange (although these phenomena will be modeled for industrial applications).

Initially, the ladle reactor contains pure iron with 500 ppm dissolved oxygen. Additional elements, namely aluminum and titanium, are introduced together during 10 s in the form of small spherical beads of diameter 4 mm. The amount of each deoxidizer is prescribed in order that all oxygen is consumed by alumina precipitation or by titanium oxide precipitation (cf. Table 2). Aluminum and titanium particles are

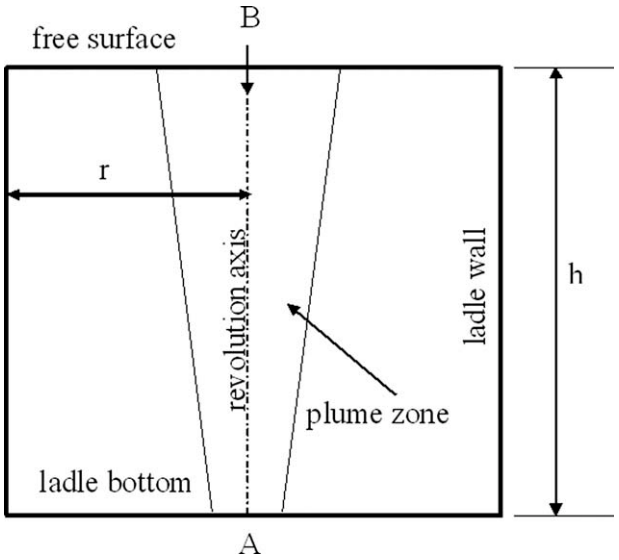

Figure 4. Sketch of the ladle reactor with its axis of revolution.

The argon bubbles are injected at the bottom center (A), and the additional elements are introduced through the slag at the top of the ladle (B).

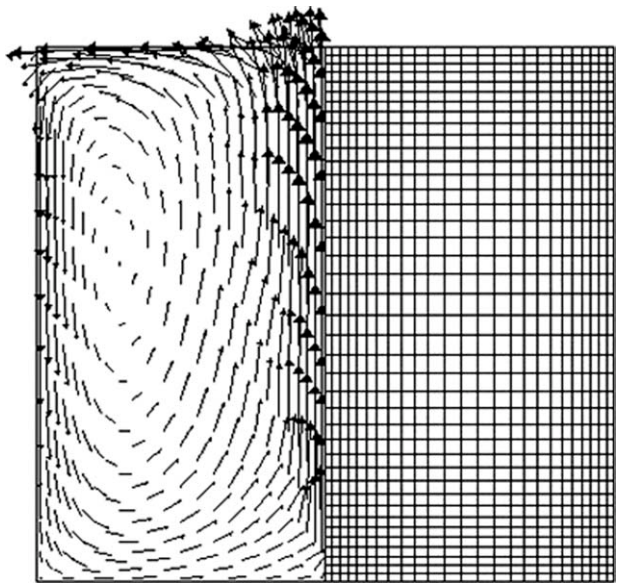

Figure 5. Fluid velocity field (left) and computational grid (right).

The maximum velocity is about 1.3 m s^{-1}.

scheduled to melt after a time delay of 1 s inside the ladle, as confirmed by a preliminary work[21] which has shown that such a melting time of 1 s is in good agreement with experimental data.

As regards the numerics, let us mention that the CFD code and the PBE solution work in double precision and that three nodes are used for each QMOM. The first six moments are chosen to track the particle distribution (m_0 to m_5).

The flow is computed using the realizable $k-\varepsilon$ turbulence model,[22] which is known to provide better performance for flows involving recirculation and prevents nonrealizability of the Reynolds stresses for flow regions where $Sk/\varepsilon > 3.7$, with S being the strain rate, k the turbulent kinetic energy, and ε the turbulent dissipation rate. This choice of turbulence model has been found to be needed in the present computations because the ratio Sk/ε has been observed to exceed the value 3.7 in the most part of the flow. The standard wall function (i.e., a logarithmic "law-of-the-wall") is used as a boundary condition at the vessel walls. It is worth noting that such a turbulence model can be used here since the liquid steel may be considered as a simple and Newtonian liquid at our working spatial and time scales[23] (its viscosity and other properties are given in Table 1). A second-order discretization scheme QUadratic Interpolation for Convective Kinematics (QUICK) is selected for the convective terms. Due to the low concentration of oxides, any effect of the particles upon the liquid steel flow can be neglected. Once the flow field has reached a steady state, it is numerically frozen and the full coupling between the numerical tools is started. All mass fractions and moments are tracked by the CFD code as passive scalars in a steady fluid flow.

Table 2. Thermo-Kinetic Data for Alumina and Titanium

	Units	Al_2O_3	TiO_2
ρ	kg m^{-3}	3.990×10^3	4.250×10^3
ΔG^0	J	$-1{,}199{,}869 + 393.212\ T$	$-645{,}874 + 224.346\ T$
V_m	$m^3\ mol^{-1}$	2.5554×10^{-5}	1.8799×10^{-5}
σ	J m^{-2}	0.1	0.1

Results

The stationary liquid flow field obtained after 180 s of stirring by argon bubbles is displayed in Figure 5. The plume zone is clearly defined with a maximum velocity near 1.3 m s^{-1}. The fluid recirculation ensures the composition homogenization and the particle transport.

The main purpose of the presented numerical model is to describe the behavior of inclusions during the ladle treatment. From now, all presented results (mass fraction, cluster size, and composition) are averaged over the entire ladle. In the plots shown in Figures 6, 7, 8, 9, 10, 11, time $t = 0$ s corresponds to the beginning of the aluminum and titanium melting, therefore all the injected particles are assumed to be dissolved in the steel at $t = 10$ s. The mass fractions of the dissolved elements and precipitated oxides are shown in Figures 6 and 7. The linear introduction of aluminum and

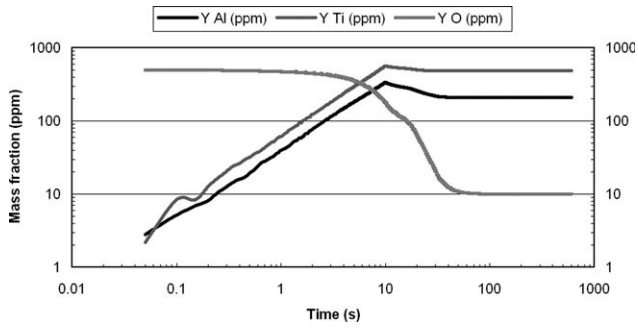

Figure 6. Time evolution of the mass fraction of dissolved elements.

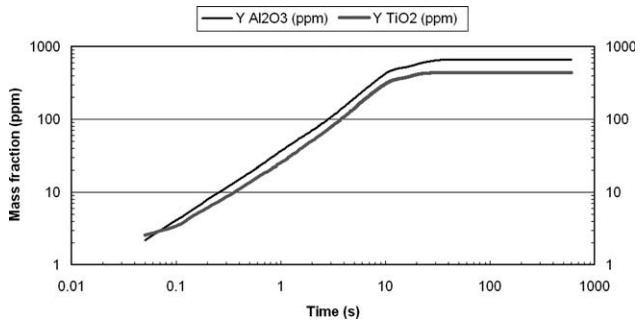

Figure 7. Time evolution of the mass fraction of precipitated oxides.

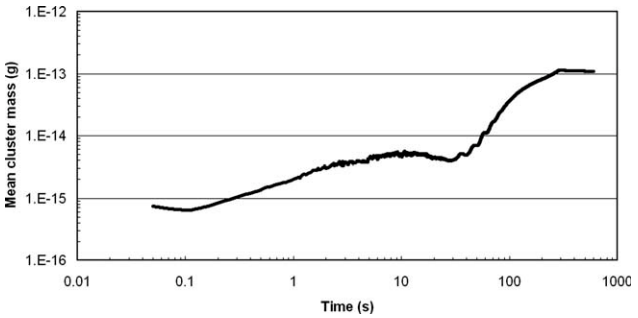

Figure 9. Time evolution of the mean mass of clusters.

titanium in Figure 6 has to be related to the linear production of oxides in Figure 7. Before 10 s, all deoxidation particles melt and they react directly with the local dissolved oxygen. After 10 s, the oxygen removal is limited by scalar transport and the ladle composition is stabilized after 100 s of chemical reaction (see Figures 6, 7, and 10). The mean Sauter diameter of clusters, $d_{32,c}$, and the mean cluster mass, M_{cluster}, are presented in Figures 8 and 9. As far as the stabilized composition appearing at the end of the simulation is considered, $d_{32,c}$ is about doubled while M_{cluster} is multiplied 10-fold; all of which is in good agreement with the calculation of particle mass using the particle diameter.

As shown by Figures 7 and 10, at the end of the simulation the clusters are composed of about 2/3 alumina and 1/3 titanium oxide, a proportion related to their respective Gibbs free energies. When aluminum and titanium are in competition for oxygen capture, thermodynamics predicts that alumina precipitates more easily than titanium oxide (see Table 2).

The mean cluster size distribution, illustrated in Figure 11 in which the weights are plotted as functions of the node abscissas, confirms the production of large inclusions (exceeding 3 μm) by consumption of small particles. The first node is divided by a factor 10 from time 100 s to 600 s. Only agglomeration due to turbulent or Stokes collisions are strong enough to explain the rise of particle diameter.

Conclusions

The cluster size and composition of solid oxide inclusions inside a liquid steel ladle of Fe-Al-Ti-O have been studied by means of an improved QMOM, called multi-QMOM. The multi-QMOM reconstructs the mean cluster size and composition and makes it possible to draw a picture of the cluster population inside the entire steel ladle. The use of $N_p + 1$ PBE/QMOM systems to predict the cluster size and composition (N_p being the number of precipitated species) requires only $N_q(N_p + 1)$ moments to be calculated and tracked by the numerical tool (where N_q is the number of QMOM nodes). To successfully run the simulation case, the standard way of taking the growth process into account has to be modified. By shifting the Dirac delta position, it is ensured that the shape of the vector of moments still describes the moments of a probability density function.

The production of large aggregates (exceeding the Kolmogorov length scale, which is of the order of 100 μm) raises the question of the validity of the turbulent aggregation kernel. Indeed, when the particle size enters the inertial domain a new turbulent aggregation kernel must be used instead of Eq. 32. This is in development and a new turbulent kernel will be implemented following the works of Abrahamson[24] and Zaichik et al.[25] Moreover, in order for the numerical predictions to assess the final cleanliness of liquid steel, appropriate extraction models will be implemented so as to simulate bubble capture, slag entrapment and wall adhesion.

As it affects mainly the buoyancy effect, the possible correlation between size and composition has been neglected, seeing that all oxides have nearly the same densities (about 4000 kg m^{-3}) in this preliminary work. To our knowledge, no study has been carried out so far regarding the effect of such a correlation. Nevertheless, we expect that the use of DQMOM would make it possible to allow for the correlation

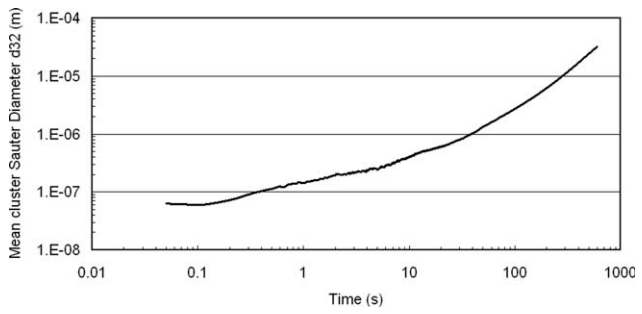

Figure 8. Time evolution of the Sauter mean diameter of clusters.

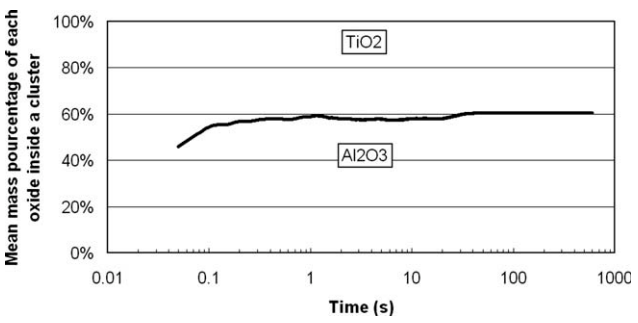

Figure 10. Predicted mass fraction of each oxide inside a cluster.

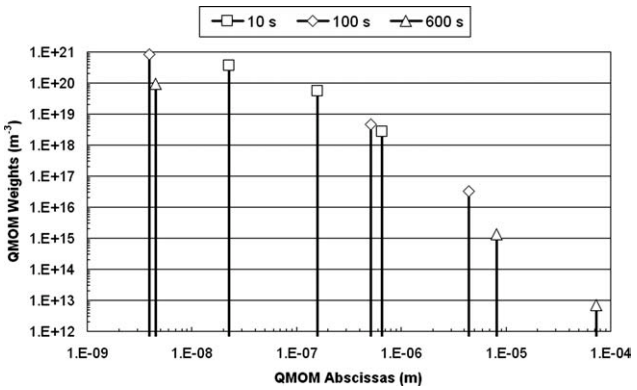

Figure 11. Illustration of the cluster size distribution at time t = 10 s, t = 100 s, and t = 600 s.

between size and composition. This new development is left for future work.

In the present state, simulations are restricted by the computational cost of the thermo-kinetic code (50 min for 90,000 cells with a time-step of 0.05 s on a quad-core bi-processor INTEL Xeon computer). Therefore, the efforts will be devoted towards the code parallelization. It is worth mentioning also that additional precipitates can easily be added into the simulation. Taking advantage of such improvements, the next important step for industrial application will be a 3D ladle study including the prediction of the production of most harmful inclusions like titanate aluminum for instance.

Acknowledgments

This project has been supported by the "Association Nationale de la Recherche Technique" (ANRT-France: Grant no. 1064/2006).

Literature Cited

1. Zhang L, Thomas BG. State of the art in evaluation and control of steel cleanliness. *ISIJ Int*. 2003;43:271–291.
2. Thuman M, Sichen D. Origins of non-metallic inclusions and their chemical development during ladle treatment. *Steel Res Int*. 2007; 79:124–131.
3. Doo WC, Kim DY, Kang SC, Yi KW. Measurement of the two-dimensional fractal dimensions of alumina clusters formed in an ultra low carbon steel melt during RH process. *ISIJ Int*. 2007; 47:1070–1072.
4. Wakow M, Sano N. Behavior of alumina inclusions just after deoxidation. *ISIJ Int*. 2007;47:627–632.
5. McGraw R. Description of aerosol dynamics by the quadrature method of moments. *Aerosol Sci Technol*. 1997;27:255–265.
6. Marchisio DL, Pikturna JT, Fox RO, Vigil DR, Barresi AA. Quadrature method of moments for population-balance equations. *AIChE J*. 2003;49:1266–1276.
7. Marchisio DL, Vigil DR, Fox RO. Quadrature method of moments for aggregation-breakage processes. *J Colloid Interf Sci*. 2003;258: 322–334.
8. Hulburt HM, Katz S. Some problems in particle technology. *Chem Eng Sci*. 1964;19:555–574.
9. Ramkrishna D. *Population Balances: Theory and Applications to Particulate Systems in Engineering*. London: Academic Press, 2000.
10. Gordon RG. Error bounds in equilibrium statistical mechanics. *J Math Phys*. 1968;9:655–663.
11. Marchisio DL, Fox RO. Solution of population balance equations using the direct quadrature method of moments. *J Aerosol Sci*. 2005;36:43–73.
12. Fox RO. Bivariate direct quadrature method of moments for coagulation and sintering of particle populations. *J Aerosol Sci*. 2006;37: 1562–1580.
13. Fox RO, Laurent F, Massot M. Numerical simulation of spray coalescence in an Eulerian framework: direct quadrature method of moments and multi-fluid method. *J Comput Phys*. 2007;227:3058–3088.
14. Lehmann J, Rocabois P, Gaye H. Kinetic model of nonmetallic inclusions precipitation during steel solidification. *J Noncryst Solids*. 2001;282:61–71.
15. Elimelech M, Gregory J, Jia X, Williams RA. *Particle Deposition and Aggregation. Measurement, Modelling and Simulation*. Woburn, MA: Butterworth-Heinemann, 1995.
16. Saffman PG, Turner JS. On the collision of drops in turbulent clouds. *J Fluid Mech*. 1956;1:16–30.
17. Cournil M, Gruy F, Gardin P, Saint-Raymond H. Modelling of solid particle aggregation dynamics in non-wetting liquid medium. *Chem Eng Process*. 2006;45:586–597.
18. Van de Ven TGM, Mason SG. The microrheology of colloidal suspensions. VII. Orthokinetic doublet formation of spheres. *Colloid Polym Sci*. 1977;255:468–479.
19. Taniguchi S, Kikuchi A, Ise T, Shoji N. Model experiment on the coagulation of inclusion particles in liquid steel. *ISIJ Int*. 1996;36 (Suppl.):S117–S120.
20. Silva LFLR, Damian RB, Lage PLC. Implementation and analysis of numerical solution of the population balance equation in CFD packages. *Comput Chem Eng*. 2008;32:2933–2945.
21. Gardin P, Domgin JF, Simonnet M, Lehmann J. Modeling of inclusion evolution in a steel ladle. *Revue Metall-Paris*. 2008;2:84–91.
22. Shih T-H, Liou WW, Shabbir A, Yang Z, Zhu J. A new k-ε eddy-viscosity model for high Reynolds number turbulent flows—model development and validation. *Comput Fluids*. 1995;24:227–238.
23. Scopigno T, Ruocco G, Sette F. Microscopic dynamics in liquid metals: the experimental point of view. *Rev Mod Phys*. 2005;77: 881–933.
24. Abrahamson J. Collision rates of small particles in a vigorously turbulent fluid. *Chem Eng Sci*. 1975;30:1371–1379.
25. Zaichik LI, Simonin O, Alipchenkov VM. Collision rates of bidisperse inertial particles in isotropic turbulence. *Phys Fluids*. 2006;18: 035110.

Manuscript received July 24, 2009, and revision received Nov. 5, 2009.